Article, Published Version

Schüttrumpf, Holger; Kortenhaus, Andreas; Pullen, Tim; Allsop, William; Bruce, Tom; Meer van der, Jentsje

Vertical and steep seawalls

Die Küste

Zur Verfügung gestellt in Kooperation mit/Provided in Cooperation with:
Kuratorium für Forschung im Küsteningenieurwesen (KFKI)

Verfügbar unter/Available at: https://hdl.handle.net/20.500.11970/101587

Vorgeschlagene Zitierweise/Suggested citation:
Schüttrumpf, Holger; Kortenhaus, Andreas; Pullen, Tim; Allsop, William; Bruce, Tom; Meer van der, Jentsje (2007): Vertical and steep seawalls. In: Die Küste 73. Heide, Holstein: Boyens. S. 130-157.

7. Vertical and step seawalls

7.1 Introduction

This chapter presents guidance for the assessment of overtopping and post-overtopping processes at vertical and steep-fronted coastal structures such as caisson and blockwork breakwaters and vertical seawalls (Fig. 7.1, Fig. 7.2). Also included are composite vertical wall structures (where the emergent part of the structure is vertical, fronted by a modest berm) and vertical structures which include a recurve/bull-nose/parapet/wave return wall as the upper part of the defence.

Large vertical breakwaters (Fig. 7.1) are almost universally formed of sand-filled concrete caissons usually resting on a small rock mound. Such caisson breakwaters may reach depths greater than 100 m, under which conditions no wave breaking at all at the wall would be expected. Conversely, older breakwaters may, out of necessity, have been constructed in shallower water or indeed, built directly on natural rock "skerries". As such, these structures may find themselves exposed to breaking wave, or "impulsive" conditions when the water depth in front of them is sufficiently low. Urban seawalls (*e.g.* Fig. 7.2) are almost universally fronted by shallow water, and are likely to be exposed to breaking or broken wave conditions, especially in areas of significant tidal range.

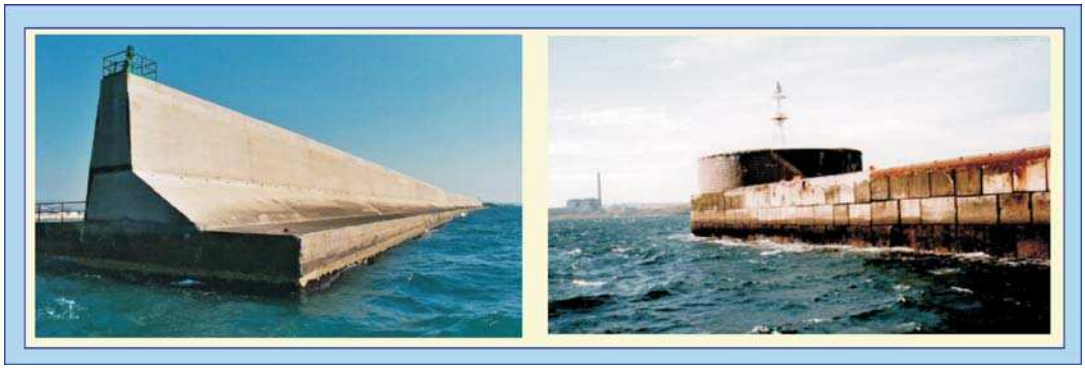

Fig. 7.1: Examples of vertical breakwaters: (left) modern concrete caisson and (right) older structure constructed from concrete blocks

Fig. 7.2: Examples of vertical seawalls: (left) modern concrete wall and (right) older stone blockwork wall

There are three principal sources of guidance on this topic preceding this manual; in the UK, the Environment Agency "Overtopping of Seawalls: Design and Assessment Manual" (EA/BESLEY, 1999); in the U.S.A., the US Army Corps of Engineers' "Coastal Engineering Manual" (CEM/BURCHARTH & HUGHES, 2002); in Japan, Goda's design charts (*e.g.* GODA, 2000). The guidance presented in this chapter builds upon that of EA/BESLEY (1999), with adjustments to many formulae based upon further testing since 1999.

For those familiar with EA/BESLEY (1999), the principal changes/additions are

- new guidance on prediction of mean and wave-by-wave overtopping to oblique wave attack under impulsive conditions (Section 7.3.4);
- extension of method for mean overtopping to account for steep (but not vertical) "battered" walls (Section 7.3.2);
- new guidance on mean overtopping under conditions when all waves break before reaching the wall (part of Section 7.3.1);
- new guidance on reduction in mean overtopping discharge due to wave return walls/parapets / recurves (Section 7.3.5);
- new guidance on "post-overtopping" processes, specifically; velocity of "throw"; landward spatial extent of overtopping, and effect of wind (Section 7.3.6)
- inclusion of summary of new evidence on scale effects for laboratory study of overtopping at vertical and steep walls (Section 7.3.7).
- minor adjustments to recommended approach for distinguishing impulsive/non-impulsive conditions (Section 7.2);
- minor adjustments to formulae for mean overtopping under impulsive conditions due to the availability of additional data, from e.g. the CLASH database (Section 7.3.1).
- all formulae are now given in terms of wave period $T_{m-1,0}$ resulting in an adjusted definition of the h^* and d^* parameters (Sections 7.2.2 and 7.2.3 respectively) in order to maintain comparability with earlier work.
- in line with convergence on the $T_{m-1,0}$ measure, formulae using wave steepness s_{op} have been adjusted to use the new preferred measure $s_{m-1,0}$ (Section 7.3.1);
- all formulae are now given explicitly in terms of basic wave and structural parameters without recourse to intermediate definitions of dimensionless overtopping discharge and freeboard parameters specific to impulsive conditions.

This chapter follows approximately the same sequence as the preceding two chapters, though certain differences should be noted. In particular, run-up is not addressed, as it is not a measure of physical importance for this class of structure – indeed it is not well-defined for cases when the wave breaks, nearly-breaks or is broken when it reaches the structure, under which conditions an up-rushing jet of water is thrown upwards.

The qualitative form of the physical processes occurring when the waves reach the wall are described in Section 7.2. Distinctions drawn between different wave/structure "regimes" are reflected in the guidance for assessment of mean overtopping discharges given in Section 7.3. The basic assessment tools are presented for plain vertical walls (Section 7.3.1), followed by subsections giving advice on how these basic tools should be adjusted to account for other commonly-occurring configurations; battered walls (Section 7.3.2); vertically composite walls (Section 7.3.3); the effect of oblique wave attack (Section 7.3.4); the effect of recurve/wave-return walls (Section 7.3.5). Scale and model effects are reviewed in Section 7.3.7. Methods to assess individual "wave by wave" overtopping volumes are presented in Section 7.4. The current knowledge and advice on post-overtopping processes including velocities, spatial distributions and post-overtopping loadings are reviewed in Section 7.5.

Principal calculation procedures are summarised in Table 7.1.

Table 7.1: Summary of principal calculation procedures for vertical structures

	Deterministic design	Probabilistic design
Discrimination – impulsive / non-impulsive regime		
plain vertical walls		Eq. 7.1
vertical composite walls		Eq. 7.2
Plain vertical walls		
non-impulsive conditions	Eq. 7.4	Eq. 7.3
impulsive conditions	Eq. 7.6	Eq. 7.5
broken wave conditions (submerged toe)	Eq. 7.8	Eq. 7.7
broken wave conditions (emergent toe)	Eq. 7.10	Eq. 7.9
Battered walls	Eq. 7.11	Eq. 7.11
Composite vertical walls	Eq. 7.13	Eq. 7.12
Oblique wave attack		
non-impulsive conditions		Eq. 7.14 & 7.15
impulsive conditions	Eq. 7.17	Eq. 7.18
Vertical walls with wave return wall / parapet		Eqs. 7.18, 7.19 & Fig. 7.20
Effect of wind		Eq. 7.20 & 7.21
Percentage of overtopping waves		Eq. 7.22 / 7.23
with oblique waves		Eqs.7.29 & 7.30
Individual overtopping volumes		Eqs.7.24 to 7.28
with oblique waves		Table 7.2
Overtopping velocities		Eq. 7.31
Spatial extent of overtopping		Fig. 7.25
Downfall pressures due to overtopped discharge		Eq. 7.32

7.2 Wave processes at walls

7.2.1 Overview

In assessing overtopping on sloping structures, it is necessary to distinguish whether waves are in the "plunging" or "surging" regime (Section 5.3.1). Similarly, for assessment of overtopping at steep-fronted and vertical structures the regime of the wave/structure interaction must be identified first, with quite distinct overtopping responses expected for each regime.

On steep walls (vertical, battered or composite), "non-impulsive" or "pulsating" conditions occur when waves are relatively small in relation to the local water depth, and of lower wave steepnesses. These waves are not critically influenced by the structure toe or approach slope. Overtopping waves run up and over the wall giving rise to (fairly) smoothly-varying loads and "green water" overtopping (Fig. 7.3).

In contrast, "impulsive" conditions (Fig. 7.4) occur on vertical or steep walls when waves are larger in relation to local water depths, perhaps shoaling up over the approach bathymetry or structure toe itself. Under these conditions, some waves will break violently against the wall with (short-duration) forces reaching 10–40 times greater than for non-impulsive conditions. Overtopping discharge under these conditions is characterised by a "violent" uprushing jet of (probably highly aerated) water.

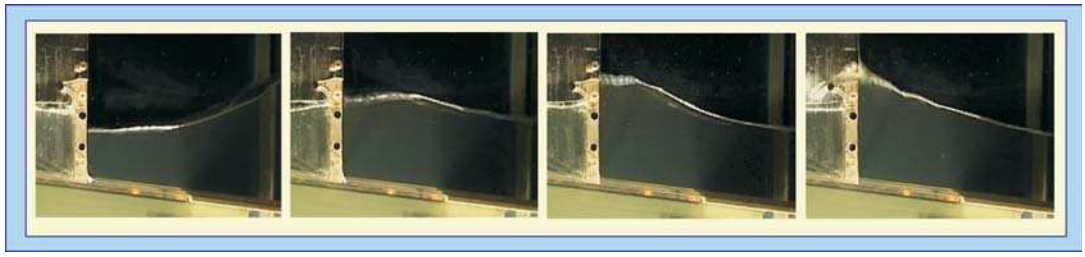

Fig. 7.3: A non-impulsive (pulsating) wave condition at a vertical wall, resulting in non-impulsive (or "green water") overtopping

Fig. 7.4: An impulsive (breaking) wave at a vertical wall, resulting in an impulsive (violent) overtopping condition

Lying in a narrow band between non-impulsive and impulsive conditions are "near-breaking" conditions where the overtopping is characterised by suddenness and a high-speed, near vertical up-rushing jet (like impulsive conditions) but where the wave has not quite broken onto the structure and so has not entrained the amount of air associated with fully impulsive conditions. This "near-breaking" condition is also known as the "flip through" condition. This conditions gives overtopping in line with impulsive (breaking) conditions and are thus not treated separately.

Many seawalls are constructed at the back of a beach such that breaking waves never reach the seawall, at least not during frequent events where overtopping is of primary importance. For these conditions, particularly for typical shallow beach slopes of less than (say) 1:30, design wave conditions may be given by waves which start breaking (possibly quite some distance) seaward of the wall. These "broken waves" arrive at the wall as a highly-aerated mass of water (Fig. 7.5), giving rise to loadings which show the sort of short-duration peak seen under impulsive conditions (as the leading edge of the mass of water arrives at the wall) but smaller in magnitude due to the high level of aeration. For cases where the depth at

Fig. 7.5: A broken wave at a vertical wall, resulting in a broken wave overtopping condition

the wall $h_s > 0$, overtopping can be assessed using the method for impulsive conditions. For conditions where the toe of the wall is emergent ($h_s \leq 0$), these methods can no longer be applied and an alternative is required (Section 7.3.1).

In order to proceed with assessment of overtopping, it is therefore necessary first to determine which is the dominant overtopping regime (impulsive or non-impulsive) for a given structure and design sea state. No single method gives a discriminator which is 100 % reliable. The suggested procedure for plain and composite vertical structures includes a transition zone in which there is significant uncertainty in the prediction of dominant overtopping regime and thus a "worst-case" is taken.

7.2.2 Overtopping regime discrimination – plain vertical walls

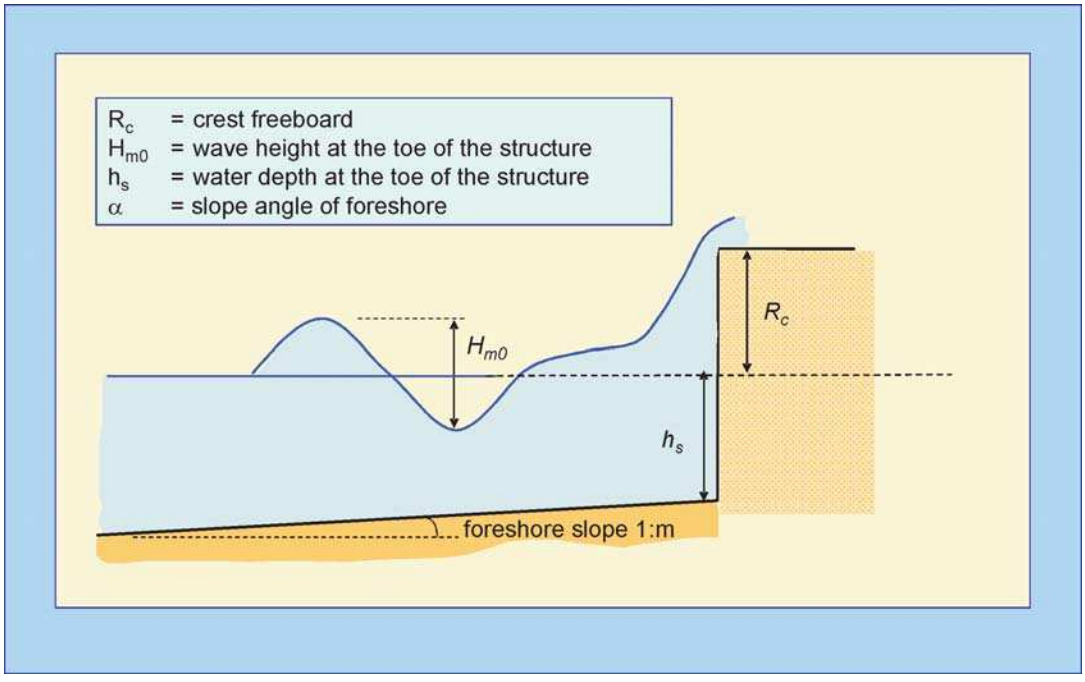

Fig. 7.6: Definition sketch for assessment of overtopping at plain vertical walls

This method is for distinguishing between impulsive and non-impulsive conditions at a vertical wall where the toe of the wall is submerged ($h_s > 0$; Fig. 7.6). When the toe of the wall is emergent ($h_s < 0$) only broken waves reach the wall.

For submerged toes ($h_s > 0$), a wave breaking or "impulsiveness" parameter, h^* is defined based on depth at the toe of the wall, h_s, and incident wave conditions inshore:

$$h_* = 1.35 \frac{h_s}{H_{m0}} \frac{2\pi h_s}{g T_{m-1,0}^2} \qquad 7.1$$

Non-impulsive (pulsating) conditions dominate at the wall when $h^* > 0.3$, and impulsive conditions occur when $h^* < 0.2$. The transition between conditions for which the overtopping response is dominated by breaking and non-breaking waves lies over $0.2 \leq h^* \leq 0.3$. In this region, overtopping should be predicted for both non-impulsive and impulsive conditions, and the larger value assumed.

7.2.3 Overtopping regime discrimination – composite vertical walls

For vertical composite walls where a berm or significant toe is present in front of the wall, an adjusted version of the method for plain vertical walls should be used. A modified "impulsiveness" parameter, d^*, is defined in a similar manner to the h^* parameter (for plain vertical walls, Section 7.2.2);

$$d_* = 1.35 \frac{d}{H_{m0}} \frac{2\pi h_s}{g T_{m-1,0}^2} \qquad 7.2$$

with parameters defined according to Fig. 7.7.

Non-impulsive conditions dominate at the wall when $d^* > 0.3$, and impulsive conditions occur when $d^* < 0.2$. The transition between conditions for which the overtopping response is dominated by breaking and non-breaking waves lies over $0.2 \leq d^* \leq 0.3$. In this region, overtopping should be predicted for both non-impulsive and impulsive conditions, and the larger value assumed.

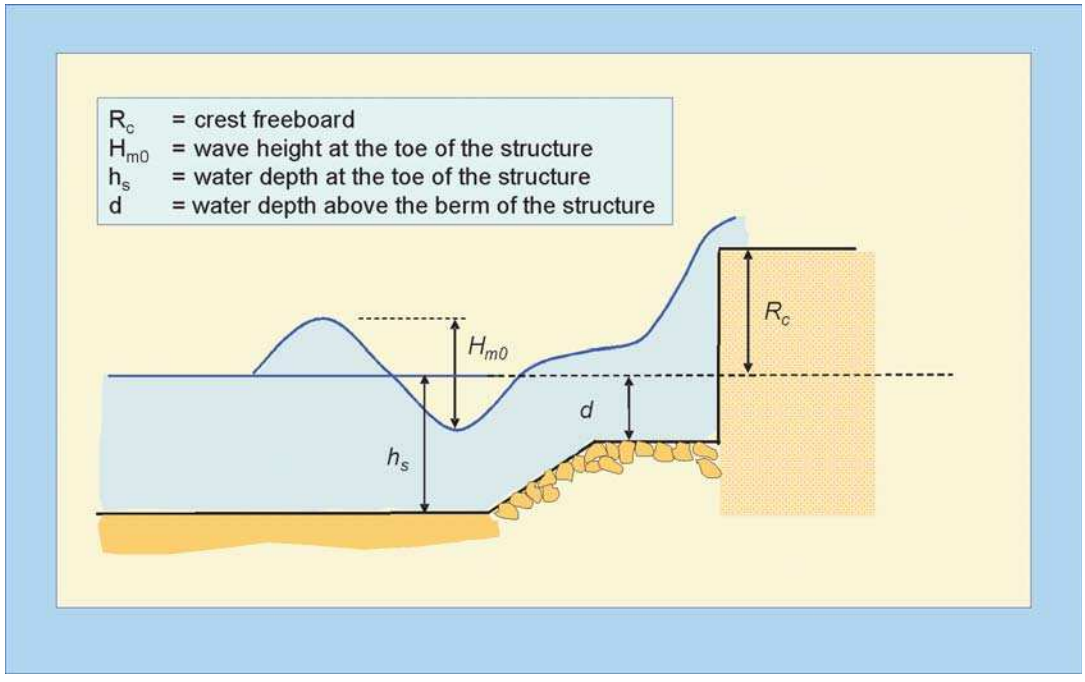

Fig. 7.7: Definition sketch for assessment of overtopping at composite vertical walls

7.3 Mean overtopping discharges for vertical and battered walls

7.3.1 Plain vertical walls

For simple vertical breakwaters under the following equations should be used:

Probabilistic design, non-impulsive conditions ($h^* > 0.3$): The mean prediction should be used for probabilistic design, or for comparison with measurements (Equation 7.3). The coefficient of 2.6 for the mean prediction has an associated standard deviation of $\sigma = 0.8$.

$$\frac{q}{\sqrt{gH_{m0}^3}} = 0.04 \exp\left(-2.6 \frac{R_c}{H_{m0}}\right) \qquad \text{valid for } 0.1 < R_c/H_{m0} < 3.5 \qquad 7.3$$

Deterministic design or safety assessment, non-impulsive conditions ($h^* > 0.3$): For deterministic design or safety assessment, the following equation incorporates a factor of safety of one standard deviation above the mean prediction:

$$\frac{q}{\sqrt{gH_{m0}^3}} = 0.04 \exp\left(-1.8 \frac{R_c}{H_{m0}}\right) \qquad \text{valid for } 0.1 < R_c/H_{m0} < 3.5 \qquad 7.4$$

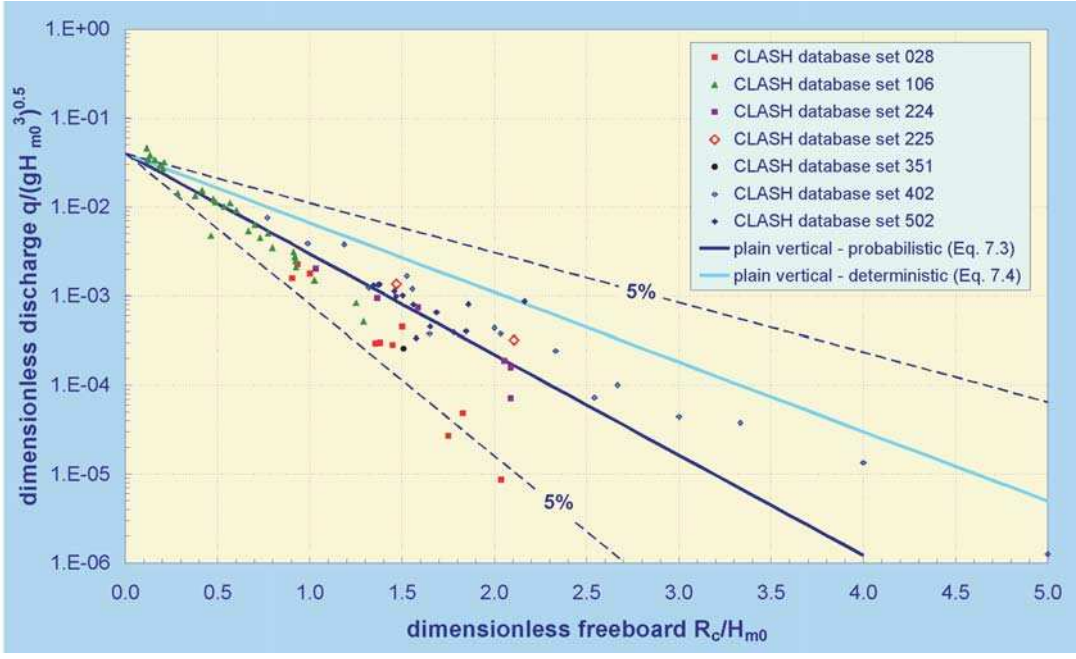

Fig. 7.8: Mean overtopping at a plain vertical wall under non-impulsive conditions (Equations 7.3 and 7.4)

Zero Freeboard: For a vertical wall under non-impulsive conditions Equation 7.5 should be used for probabilistic design and for prediction and comparison of measurements (Fig. 5.13) SMID (2001).

$$\frac{q}{\sqrt{gH_{m0}^3}} = 0.062 \pm 0.0062 \qquad \text{valid for } R_c/H_{m0} = 0 \qquad 7.5$$

For deterministic design or safety assessment it is recommended to increase the average overtopping discharge in Equation 7.5 by one standard deviation.

No data are available for impulsive overtopping at zero freeboard at vertical walls.

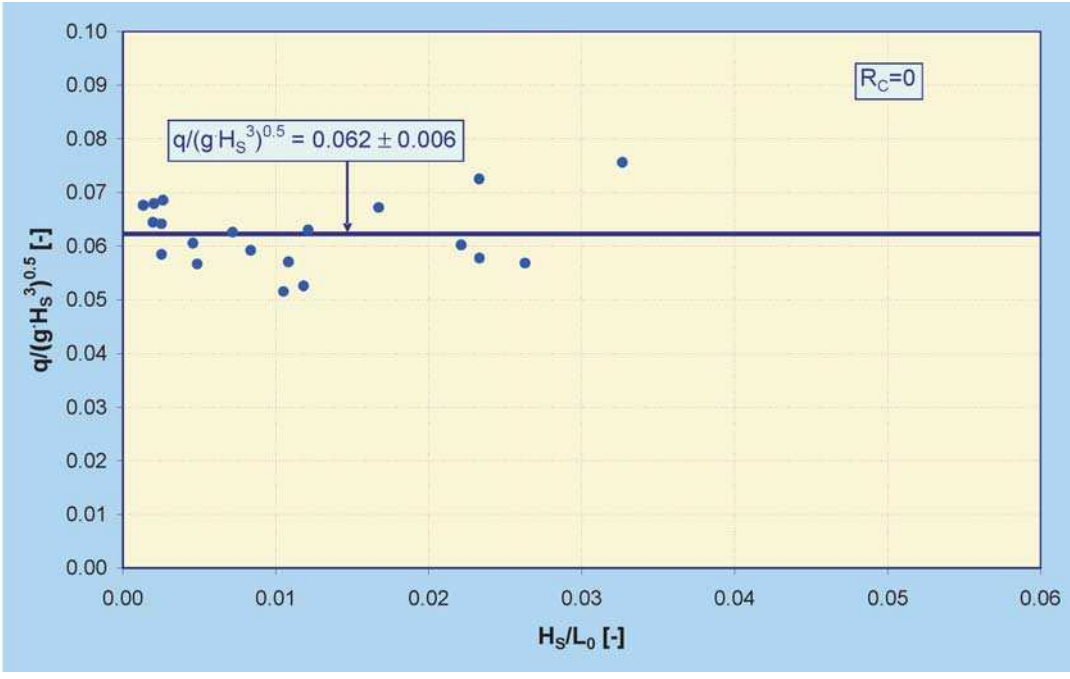

Fig. 7.9: Dimensionless overtopping discharge for zero freeboard (SMID, 2001)

Probabilistic design, impulsive conditions ($h_* \leq 0.2$): The mean prediction should be used for probabilistic design, or for comparison with measurements (Equation 7.6). The scatter *in the logarithm* of the data about the mean prediction is characterised by a standard deviation of *c.* 0.37 (*i.e. c.* 68 % of predictions lie within a range of ×/÷ 2.3).

$$\frac{q}{h_*^2\sqrt{gh_s^3}} = 1.5\times10^{-4}\left(h_*\frac{R_c}{H_{m0}}\right)^{-3.1} \qquad \text{valid over } 0.03 < h_*\frac{R_c}{H_{m0}} < 1.0 \qquad 7.6$$

Deterministic design or safety assessment, impulsive conditions ($h_* \leq 0.2$): For deterministic design or safety assessment, the following equation incorporates a factor of safety of one standard deviation above the mean prediction:

$$\frac{q}{h_*^2\sqrt{gh_s^3}} = 2.8\times10^{-4}\left(h_*\frac{R_c}{H_{m0}}\right)^{-3.1} \qquad \text{valid over } 0.03 < h_*\frac{R_c}{H_{m0}} < 1.0 \qquad 7.7$$

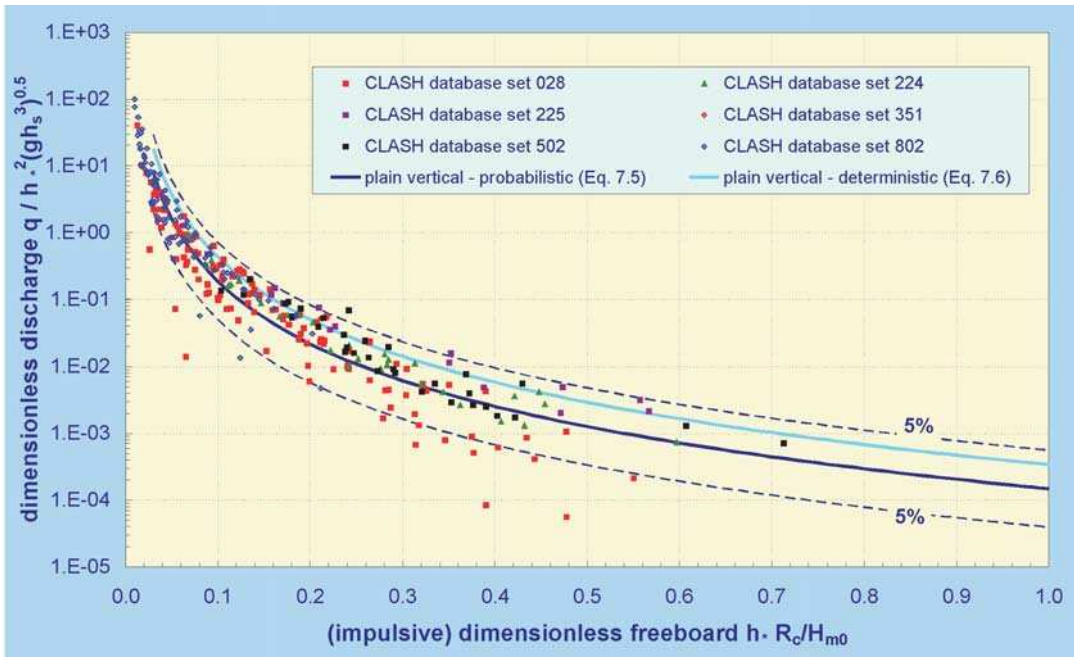

Fig. 7.10: Mean overtopping at a plain vertical wall under impulsive conditions (Equations 7.6 and 7.7)

For $R_h < 0.02$ arising from h_s reducing to very small depths (as opposed to from small relative freeboards) there is evidence supporting an adjustment downwards of the predictions of the impulsive formulae due to the observation that only broken waves arrive at the wall (BRUCE et al., 2003). For probabilistic design or comparison with measurements, the mean prediction should be used (Equation 7.8). The scatter in the logarithm of the data about the mean prediction is characterised by a standard deviation of *c.* 0.15 (*i.e. c.* 68 % of predictions lie within a range of ×/÷ 1.4).

$$\frac{q}{h_*^2\sqrt{gh_s^3}} = 2.7 \times 10^{-4}\left(h_*\frac{R_c}{H_{m0}}\right)^{-2.7} \quad \text{valid for } h_*\frac{R_c}{H_{m0}} < 0.02\text{; broken waves} \qquad 7.8$$

For **deterministic design or safety assessment,** the following equation incorporates a factor of safety of one standard deviation (in the multiplier) above the mean prediction:

$$\frac{q}{h_*^2\sqrt{gh_s^3}} = 3.8 \times 10^{-4}\left(h_*\frac{R_c}{H_{m0}}\right)^{-2.7} \quad \text{valid for } h_*\frac{R_c}{H_{m0}} < 0.02\text{; broken waves} \qquad 7.9$$

For $0.02 < h_* R_c / H_{m0} < 0.03$, there appears to be a transition between Equation 7.7 (for "normal" impulsive conditions) and Equation 7.8 (for conditions with only broken waves). There is however insufficient data upon which to base a firm recommendation in this range. It is suggested that Equation 7.7 is used down to $h_* R_c / H_{m0} = 0.02$ unless it is clear that only broken waves will arrive at the wall, in which case Equation 7.8 could be used. Formulae for these low $h_* R_c / H_{m0}$ conditions are shown in Fig. 7.11.

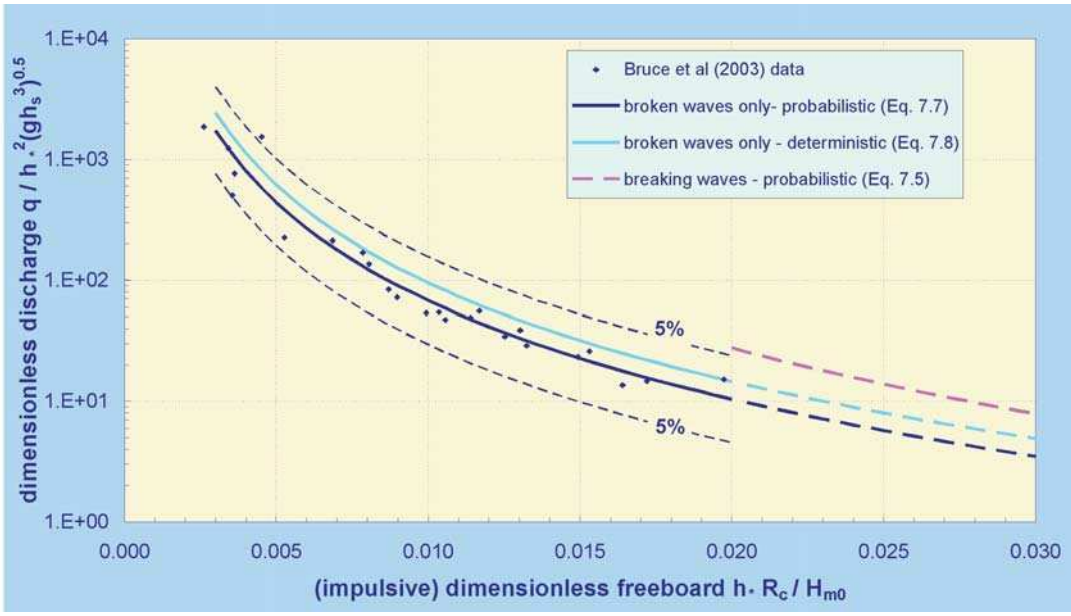

Fig. 7.11: Mean overtopping discharge for lowest $h^* R_c / H_{m0}$ (for broken waves only arriving at wall) with submerged toe ($h_s > 0$). For $0.02 < h^* R_c / H_{m0} < 0.03$, overtopping response is ill-defined – lines for both impulsive conditions (extrapolated to lower $h^* R_c / H_{m0}$) and broken wave only conditions (extrapolated to higher $h^* R_c / H_{m0}$) are shown as dashed lines over this region

Data for configurations where the toe of the wall is emergent (*i.e.* at or above still water level, $h_s \leq 0$) is limited. The only available study suggests an adaptation of a prediction equation for plunging waves on a smooth slope may be used, but particular caution should be exercised in any extrapolation beyond the parameter ranges of the study, which only used a relatively steep (m =10) foreshore slope.

For **probabilistic design or comparison with measurements,** the mean prediction should be used (Equation 7.10) should be used. The standard deviation associated with the exponent coefficient (–2.16) is *c.* 0.21.

$$\frac{q}{\sqrt{gH_{m0,deep}^3}} \cdot \sqrt{m s_{m-1,0}} = 0.043 \exp\left(-2.16 m s_{m-1,0}^{0.33} \frac{R_c}{H_{m0,deep}}\right) \qquad 7.10$$

valid for $2.0 < m s_{m-1,0}^{0.33} \frac{R_c}{H_{m0,deep}} < 5.0$; $0.55 \leq R_c/H_{m0,deep}$

$s_{m-1,0} \geq 0.02$ 5; Note – data only available for m =10 (*i.e.* 1:10 foreshore slope)

For **deterministic design or safety assessment,** Equation 7.11 incorporates a factor of safety of one standard deviation (in the exponent) above the mean prediction.

$$\frac{q}{\sqrt{gH_{m0,deep}^3}} \cdot \sqrt{m s_{m-1,0}} = 0.043 \exp\left(-1.95 m s_{m-1,0}^{0.33} \frac{R_c}{H_{m0,deep}}\right) \qquad 7.11$$

valid for $2.0 < m s_{m-1,0}^{0.33} \frac{R_c}{H_{m0,deep}} < 5.0$; $0.55 \leq R_c/H_{m0,deep} \leq 1.6$;

$s_{m-1,0} \geq 0.02$ 5; NB – data only available for m = 10 (*i.e.* 1:10 foreshore slope)

Equations 7.10 and 7.11 for overtopping under emergent toe conditions are illustrated in Fig. 7.12. It should be noted that this formula is based upon a limited dataset of small-scale tests with 1:10 foreshore only and should not be extrapolated beyond the ranges tested (foreshore slope 1:m = 0.1; $s_{op} \geq 0.025$; $0.55 \leq R_c/H_{m0,deep} \leq 1.6$).

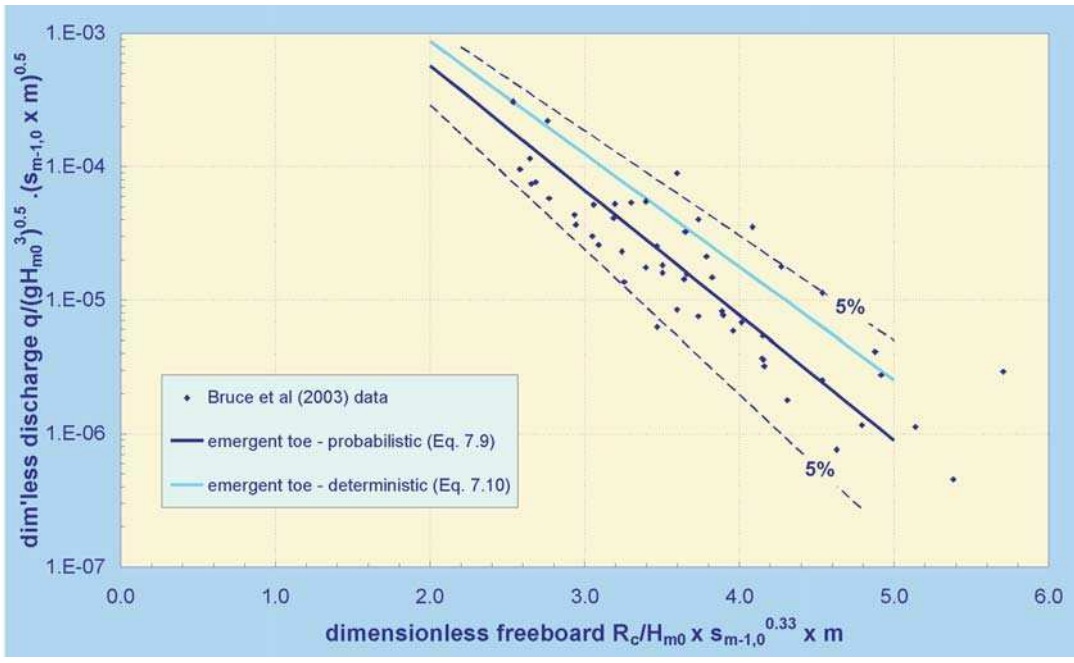

Fig. 7.12: Mean overtopping discharge with emergent toe ($h_s < 0$)

7.3.2 Battered walls

Near-vertical walls with 10:1 and 5:1 batters are found commonly for older UK seawalls and breakwaters (*e.g.* Fig. 7.13).

Mean overtopping discharges for battered walls under impulsive conditions are slightly in excess of those for a vertical wall over a wide range of dimensionless freeboards. Multiplying factors are given in Equation 7.12 (plotted in Fig. 7.14).

$$\begin{aligned} &\text{10:1 battered wall:} && q_{10:1\ batter} = q_{vertical} \times 1.3 \\ &\text{5:1 battered wall:} && q_{5:1\ batter} = q_{vertical} \times 1.9 \end{aligned} \qquad 7.12$$

where $q_{vertical}$ is arrived at from Equation 7.6 (for probabilistic design) or Equation 7.7 (for deterministic design). The uncertainty in the final estimated overtopping discharge can be estimated as per the plain vertical cases.

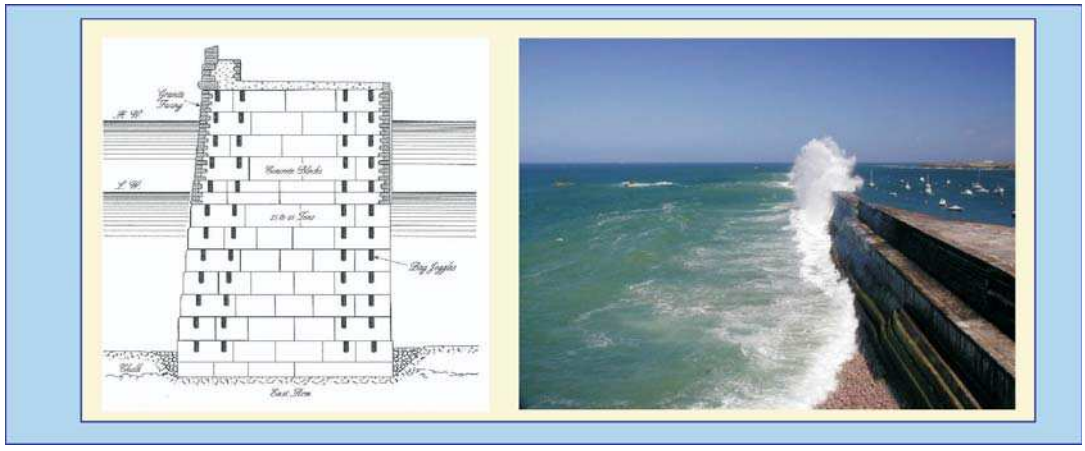

Fig. 7.13: Battered walls: typical cross-section (left), and Admiralty Breakwater, Alderney Channel Islands (right, courtesy G. MÜLLER)

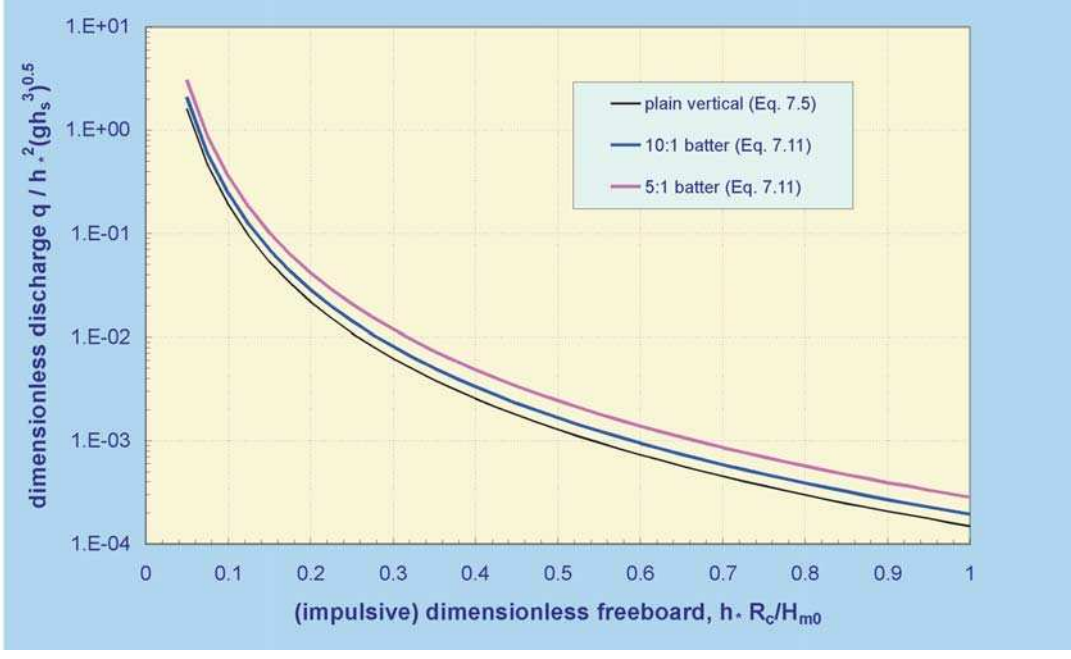

Fig. 7.14: Overtopping for a 10:1 and 5:1 battered walls

No dataset is available to indicate an appropriate adjustment under non-impulsive conditions. Given that these battered structures are generally older structures in shallower water, it is likely that impulsive conditions are possible at most, and will form the design case.

7.3.3 Composite vertical walls

It is well-established that a relatively small toe berm can change wave breaking characteristics, thus substantially altering the type and magnitude of wave loadings (e.g. (OUMERACI et al., 2001). Many vertical seawall walls may be fronted by rock mounds with the intention

of protecting the toe of the wall from scour. The toe configuration can vary considerably, potentially modifying the overtopping behaviour of the structure. Three types of mound can be identified

1. Small toe mounds which have an insignificant effect on the waves approaching the wall – here the toe may be ignored and calculations proceed as for simple vertical (or battered) walls.
2. Moderate mounds, which significantly affect wave breaking conditions, but are still below water level. Here a modified approach is required.
3. Emergent mounds in which the crest of the armour protrudes above still water level. Prediction methods for these structures may be adapted from those for crown walls on a rubble mound (Section 6.3.5).

For assessment of mean overtopping discharge at a composite vertical seawall or breakwater, the overtopping regime (impulsive/non-impulsive) must be determined – see Section 7.2.3.

When non-impulsive conditions prevail, overtopping can be predicted by the standard method given previously for non-impulsive conditions at plain vertical structures, Equation 7.3.

For conditions determined to be impulsive, a modified version of the impulsive prediction method for plain vertical walls is recommended, accounting for the presence of the mound by use of d and d^*.

For **probabilistic design or comparison with measurements,** the mean prediction (Equation 7.13) should be used. The scatter *in the logarithm* of the data about the mean prediction is characterised by a standard deviation of *c.* 0.28 (*i.e. c.* 68 % of predictions lie within a range of ×/÷ 1.9).

$$\frac{q}{d_*^2\sqrt{gh_s^{\,3}}} = 4.1\times10^{-4}\left(d_*\frac{R_c}{H_{m0}}\right)^{-2.9} \qquad 7.13$$

$$\text{valid for } 0.05 < d_*\frac{R_c}{H_{m0}} < 1.0 \text{ and } h_* < 0.3$$

For **deterministic design or safety assessment,** Equation 7.14 incorporates a factor of safety of one standard deviation (in the constant multiplier) above the mean prediction.

$$\frac{q}{d_*^2\sqrt{gh_s^{\,3}}} = 7.8\times10^{-4}\left(d_*\frac{R_c}{H_{m0}}\right)^{-2.6} \qquad 7.14$$

$$\text{valid for } 0.05 < d_*\frac{R_c}{H_{m0}} < 1.0 \text{ and } h_* < 0.3$$

7.3.4 Effect of oblique waves

Seawalls and breakwaters seldom align perfectly with incoming waves. The assessment methods presented thus far are only valid for shore-normal wave attack. In this subsection, advice on how the methods for shore-normal wave attack (obliquity $\beta = 0°$) should be adjusted for oblique wave attack.

This chapter extends the existing design guidance for impulsive wave attack from perpendicular to oblique wave attack. As for zero obliquity, overtopping response depends

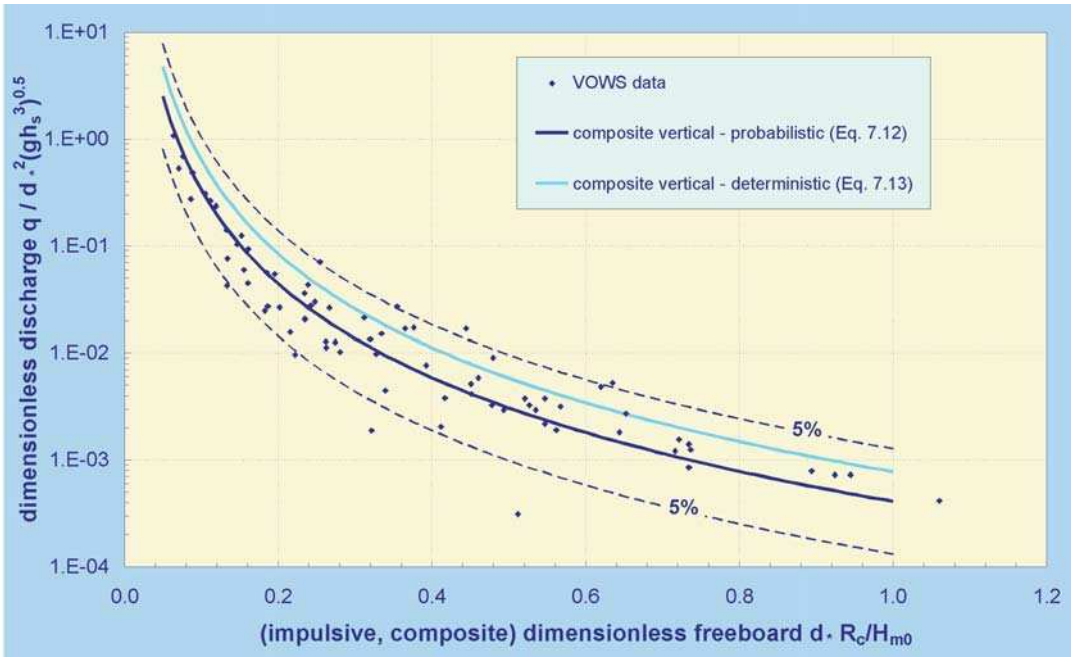

Fig. 7.15: Overtopping for composite vertical walls

critically upon the physical form (or "regime") of the wave/wall interaction – non-impulsive; impulsive or broken. As such, the first step is to use the methods given in Section 7.2 to determine the form of overtopping for shore-normal (zero obliquity). Based upon the outcome of this, guidance under "non-impulsive conditions" or "impulsive conditions" should be followed.

For non-impulsive conditions, an adjusted version of Equation 7.3 should be used (Equation 7.15):

$$\frac{q}{\sqrt{gH_{m0}^3}} = 0.04 \exp\left(-\frac{2.6}{\gamma}\frac{R_c}{H_{m0}}\right) \qquad 7.15$$

where γ is the reduction factor for angle of attack and is given by

$$\gamma = 1 - 0.0062\beta \quad \text{for } 0^0 < \beta < 45^o$$
$$\gamma = 0.72 \quad \text{for } \beta \geq 45^o \qquad 7.16$$

and β is the angle of attack relative to the normal, in degrees.

For conditions that would be identified as impulsive for normal ($\beta = 0°$) wave attack, a more complex picture emerges (NAPP et al., 2004). Diminished incidence of impulsive overtopping is observed with increasing obliquity (angle β) of wave attack. This results not only in reductions in mean discharge with increasing β but also, for $\beta \geq 60°$, a switch back over to the functional form observed for non-impulsive conditions (*i.e.* a move away from a power-law decay such as Equation 7.6 to an exponential one such as Equation 7.3).

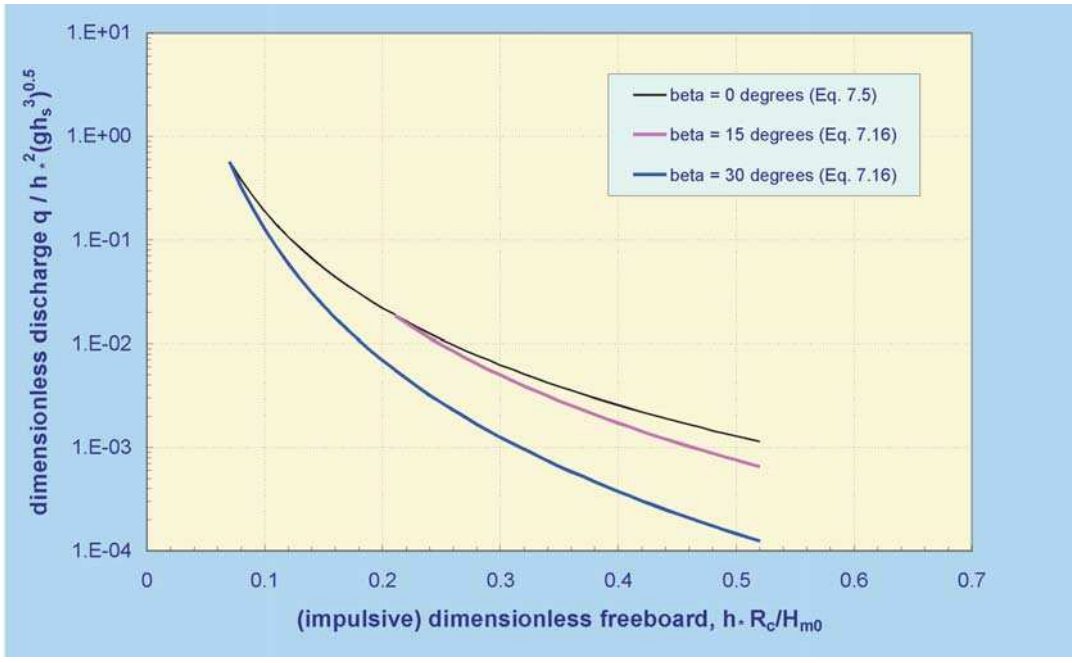

Fig. 7.16: Overtopping of vertical walls under oblique wave attack

For **probabilistic design or comparison with measurements,** the mean predictions should be used (Equation 7.17) should be used. Data only exist for the discrete values of obliquity listed.

for β = 15° ; $h_* \frac{R_c}{H_{m0}} \geq 0.2$	$\frac{q}{h_*^2\sqrt{gh_s^3}} = 5.8\times10^{-5}\left(h_* \frac{R_c}{H_{m0}}\right)^{-3.7}$	
for β = 15° ; $h_* \frac{R_c}{H_{m0}} < 0.2$	as per impulsive β = 0° (Eq. 7.6).	
for β = *30* °; $h_* \frac{R_c}{H_{m0}} \geq 0.07$	$\frac{q}{h_*^2\sqrt{gh_s^3}} = 8.0\times10^{-6}\left(h_* \frac{R_c}{H_{m0}}\right)^{-4.2}$	7.17
for β = *60* °; $h_* \frac{R_c}{H_{m0}} \geq 0.07$	as per non-impulsive β=60° (Eq. 7.16).	

Significant spatial variability of overtopping volumes along the seawall under oblique wave attack are observed/measured in physical model studies. For **deterministic design**, Equation 7.18 should be used, as these give estimates of the "worst case" conditions at locations along the wall where the discharge is greatest.

for β = 15^0 ; $h_* \frac{R_c}{H_{m0}} \geq 0.2$	as per impulsive β = 0° (Eq.7.7)	
for β = *30* ^{0}; $h_* \frac{R_c}{H_{m0}} \geq 0.07$	as per impulsive β = 15° (Eq.7.17)	7.18
for β = *60* ^{0}; $h_* \frac{R_c}{H_{m0}} \geq 0.07$	as per non-impulsive β = 0° (Eq.7.4)	

7.3.5 Effect of bullnose and recurve walls

Designers of vertical seawalls and breakwaters have often included some form of seaward overhang (*recurve/parapet/wave return wall/bullnose*) as part of the structure with the design motivation of reducing wave overtopping by deflecting back seaward uprushing water (eg Fig. 7.18). The mechanisms determining the effectiveness of a recurve are complex and not yet fully described. The guidance presented here is based upon physical model studies (KORTENHAUS et al., 2003; PEARSON et al., 2004).

Parameters for the assessment of overtopping at structures with bullnose/recurve walls are shown in Fig. 7.19.

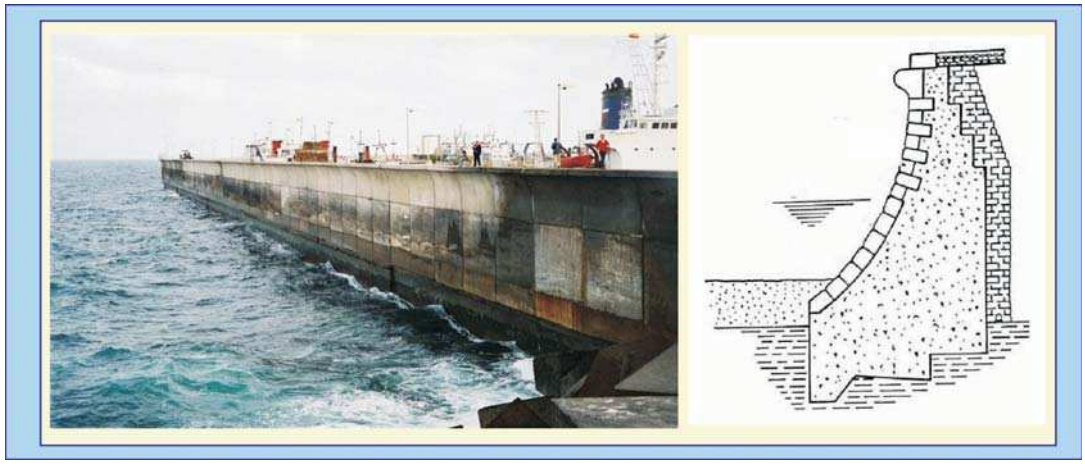

Fig. 7.17: An example of a modern, large vertical breakwater with wave return wall (left) and cross-section of an older seawall with recurve (right)

Fig. 7.18: A sequence showing the function of a parapet/wave return wall in reducing overtopping by redirecting the uprushing water seaward (back to right)

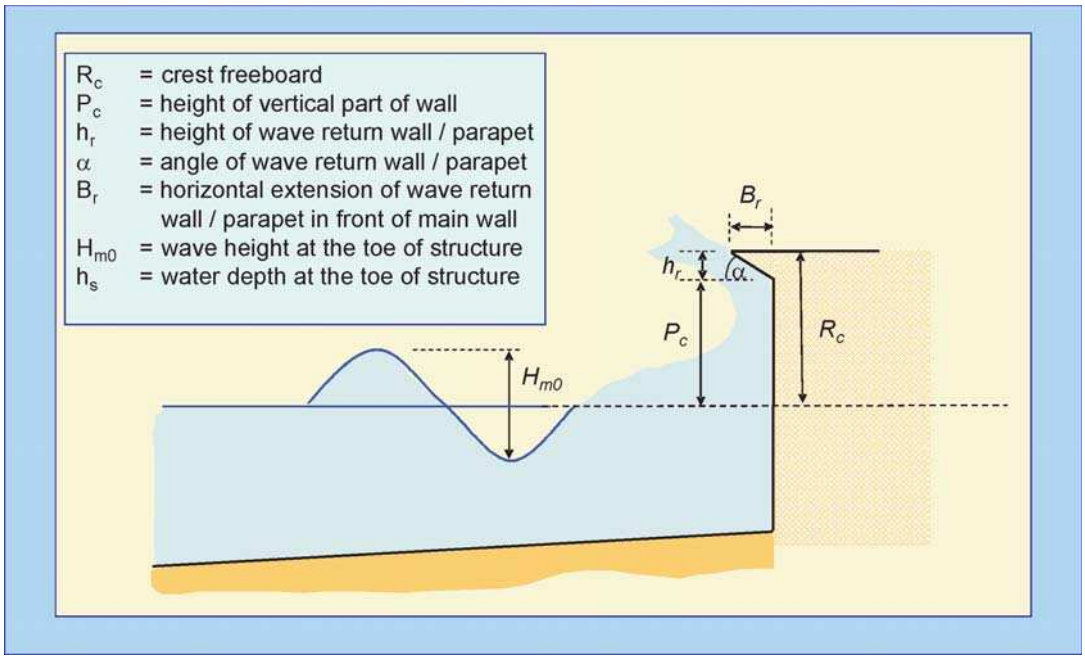

Fig. 7.19: Parameter definitions for assessment of overtopping at structures with parapet/wave return wall

Two conditions are distinguished;

- the familiar case of the parapet/bullnose/recurve overhanging seaward ($\alpha < 90°$), and
- the case where a wall is chamfered backwards at the crest (normally admitting *greater* overtopping ($\alpha > 90°$).

For the latter, chamfered wall case, Cornett influence factors γ should be applied to Franco's equation for non-impulsive mean discharge (Equation 7.19) with a value of γ selected as shown (CORNETT et al., 1999).

$$\frac{q}{\left(gH_{m0}^3\right)^{0.5}} = 0.2\exp\left(-\frac{4.3}{\gamma}\frac{R_c}{H_{m0}}\right) \qquad 7.19$$

$\gamma = 1.01$ for $\alpha = 120°$
$\gamma = 1.13$ for $\alpha = 135°$
$\gamma = 1.07$ for $\alpha = 150°$

For the familiar case of overhanging parapet/recurve/bullnose, the effectiveness of the recurve/parapet in reducing overtopping is quantified by a factor k defined as

$$k = \frac{q_{\text{with\_recurve}}}{q_{\text{without\_recurve}}} \qquad 7.20$$

The decision chart in Fig. 7.20 can then be used to arrive at a value of *k*, which in turn can be applied by multiplication to the mean discharge predicted by the most appropriate method for the plain vertical wall (with the same R_c, h_s etc.). The decision chart shows three levels of decision;

- whether the parapet is angled seaward or landward;
- if seaward ($\alpha < 90°$), whether conditions are in the small (left box), intermediate (middle box) or large (right box) reduction regimes;
- if in the regime of largest reductions (greatest parapet effectiveness; $R_c/H_{m0} \geq R_0^* + m^*$), which of three further sub-regimes (for different R_c/h_s) is appropriate.

Given the level of scatter in the original data and the observation that the methodology is not securely founded on the detailed physical mechanisms/processes, it is suggested that it is impractical to design for $k < 0.05$, i.e. reductions in mean discharges by factors of greater than 20 cannot be predicted with confidence. If such large (or larger) reductions are required, a detailed physical model study should be considered.

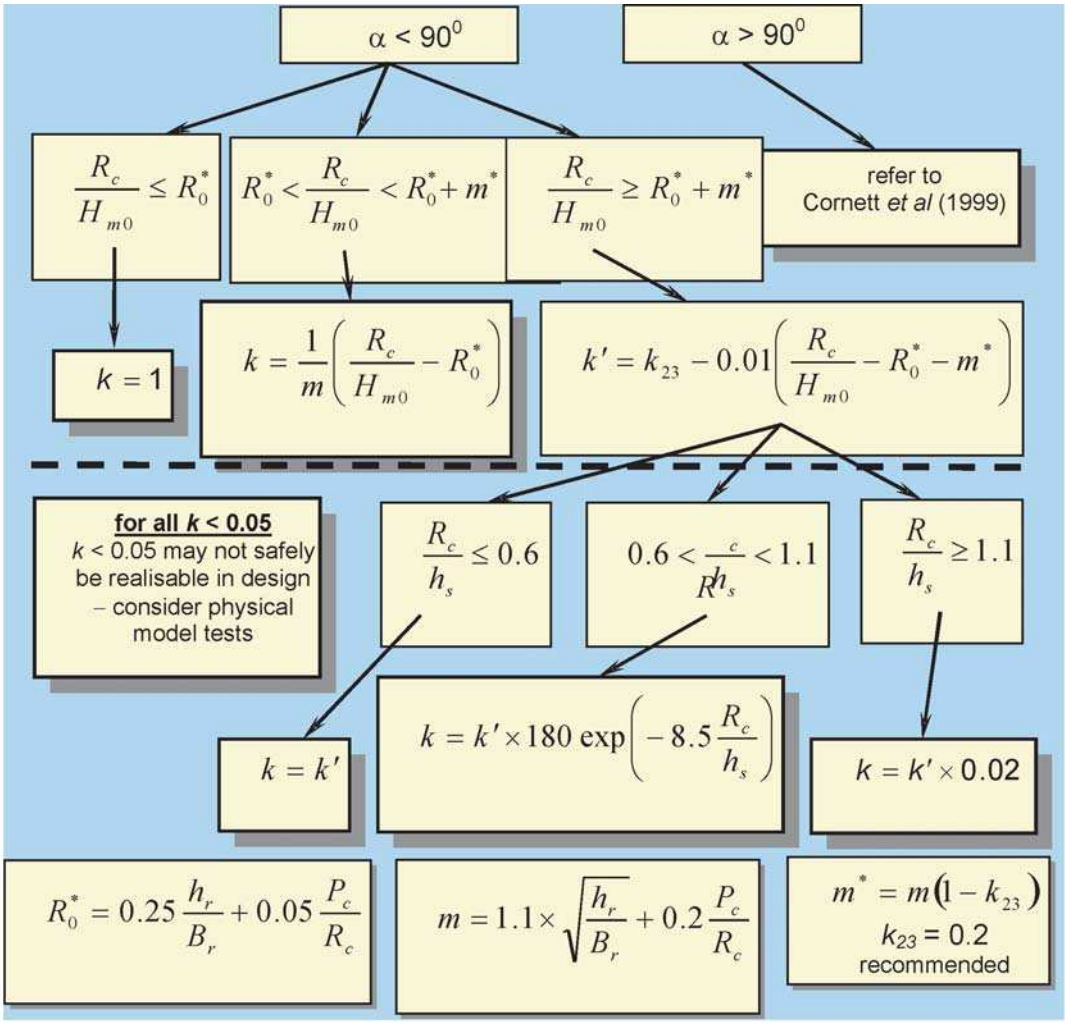

Fig. 7.20: "Decision chart" summarising methodology for tentative guidance. Note that symbols R_0^*, k_{23}, m and m^* used (only) at intermediate stages of the procedure are defined in the lowest boxes in the figure. Please refer to text for further explanation

7.3.6 Effect of wind

Wind may affect overtopping processes and thus discharges by:

- changing the shape of the incident wave crest at the structure resulting in a possible modification of the dominant regime of wave interaction with the wall;
- blowing up-rushing water over the crest of the structure (for an onshore wind, with the reverse effect for an offshore wind) resulting in possible modification of mean overtopping discharge and wave-by-wave overtopping volumes;
- modifying the physical form of the overtopping volume or jet, especially in terms of its aeration and break-up resulting in possible modification to post-overtopping characteristics such as throw speed, landward distribution of discharge and any resulting post-overtopping loadings (e.g. downfall pressures).

The modelling of any of these effects in small-scale laboratory tests presents very great difficulties owing to fundamental barriers to the simultaneous scaling of the wave-structure and water-air interaction processes. Very little information is available to offer guidance on effect (1) – the reshaping of the incident waves. Comparisons of laboratory and field data (both with and without wind) have enabled some upper (conservative) bounds to be placed upon effect (2) – the intuitive wind-assistance in "pushing" of up-rushing water landward across the crest. These are discussed immediately below. Discussion of effect (3) – modification to "post-overtopping" processes – is reserved for Sections 7.5.3 and 7.5.4 (on distributions and downfalling pressures respectively).

For vertical structures, several investigations on vertical structures have suggested different adjustment factors f_{wind} ranging from 30 % to 40 % to up to 300 % (Fig. 7.21) either using a paddle wheel or large fans to transport uprushing water over the wall.

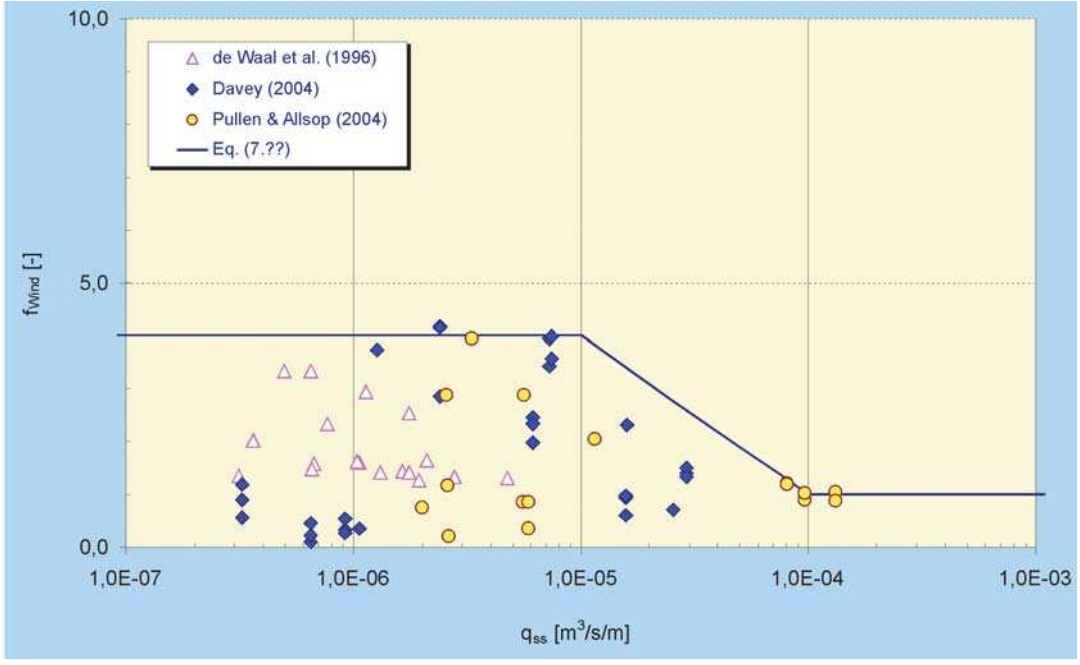

Fig. 7.21: Wind adjustment factor f_{wind} plotted over mean overtopping rates q_{ss}

When these tests were revisited a simple adjustment factor was proposed for the mean discharge based upon small-scale tests q_{ss}, which is already scaled up by appropriate scaling to full-scale (see also de ROUCK et al., 2005).

$$f_{wind} = \begin{cases} 4.0 & \text{for } q_{ss} \le 10^{-5}\ \text{m}^3/\text{s/m} \\ 1.0 + 3.(-\log q_{ss} - 4) & \text{for } 10^{-5} < q_{ss} < 10^{-4}\ \text{m}^3/\text{s/m} \\ 1.0 & \text{for } q_{ss} \ge 10^{-4}\ \text{m}^3/\text{s/m} \end{cases} \qquad 7.21$$

From Equation 7.21 it becomes clear that the influence of wind only gets important for very low overtopping rates below q_{ss} = 0.1 l/s/m. Hence, in many practical cases, the influence of wind may be disregarded. The mean overtopping discharge including wind becomes

$$q_{\text{with wind}} = f_{\text{wind}} \times q_{\text{ss}} \qquad 7.22$$

7.3.7 Scale and model effect corrections

Tests in a large-scale wave channel (Fig. 7.22) and field measurements (Fig. 7.23) have demonstrated that with the exception of wind effect (Section 7.3.6), results of overtopping measurements in small-scale laboratory studies may be securely scaled to full-scale under non-impulsive and impulsive overtopping conditions (PEARSON et al., 2002; PULLEN et al., 2004).

No information is yet available on the scaling of small-scale data under conditions where broken wave attack dominates. Comparison of measurements of wave loadings on vertical structures under broken wave attack at small-scale and in the field suggests that prototype loadings will be *over-estimated* by small-scale tests in the presence of highly-aerated broken waves. Thus, although the methods presented for the assessment of overtopping discharges under broken wave conditions given in Section 7.3.1 have not been verified at large-scale or in the field, any scale correction is expected to give a *reduction* in predicted discharge.

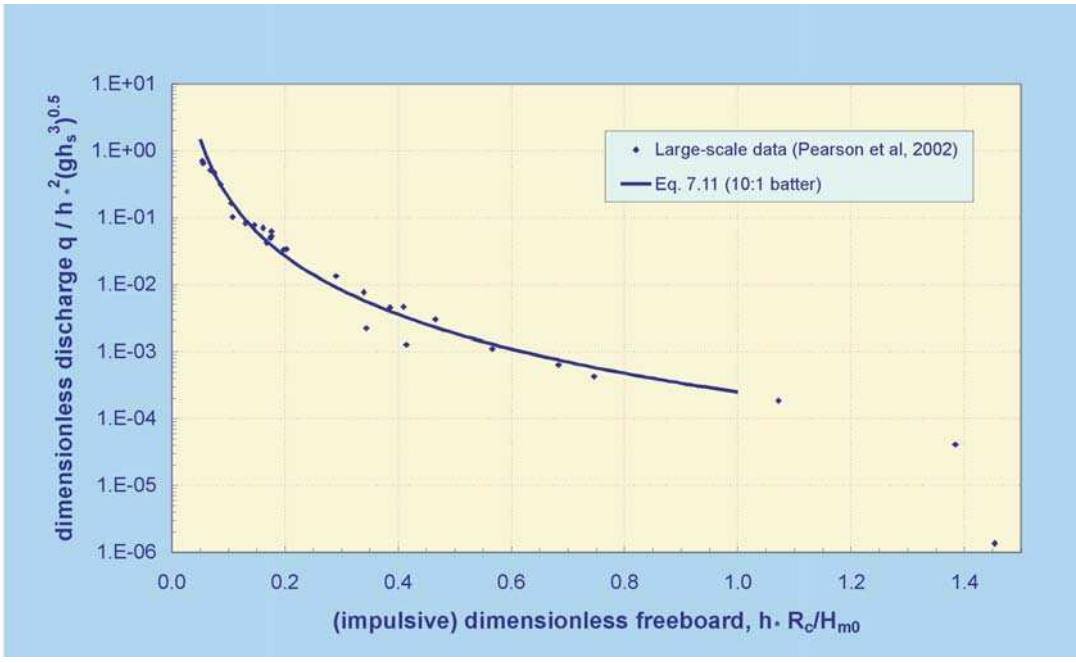

Fig. 7.22: Large-scale laboratory measurements of mean discharge at 10:1 battered wall under impulsive conditions showing agreement with prediction line based upon small-scale tests (Equation 7.12)

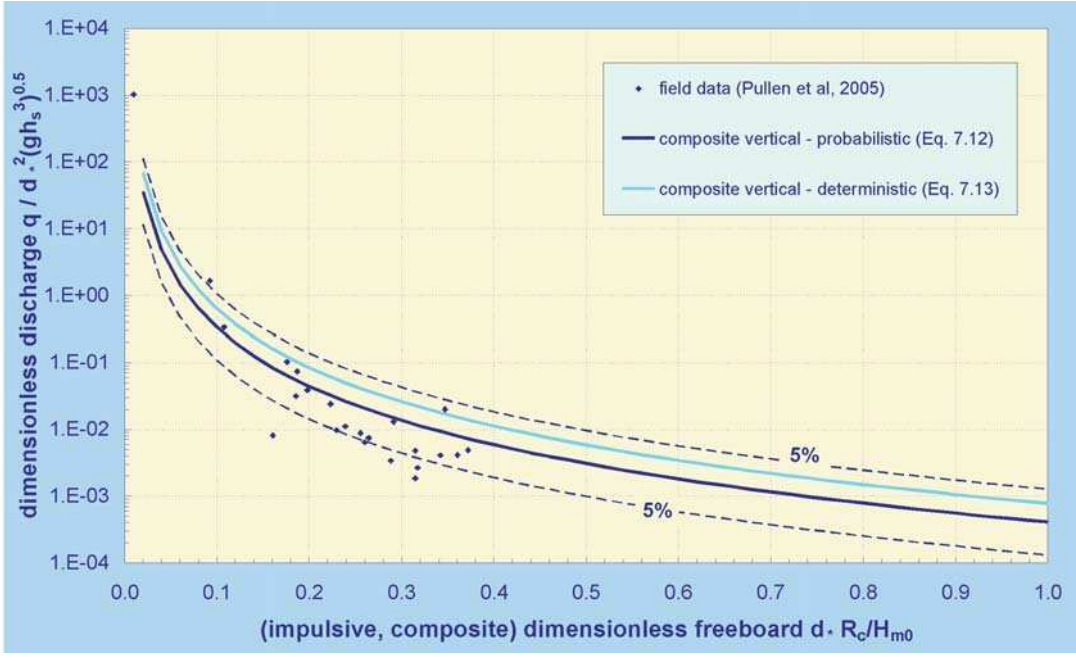

Fig. 7.23: Results from field measurements of mean discharge at Samphire Hoe, UK, plotted together with Equation 7.13

7.4 Overtopping volumes

7.4.1 Introduction

While the prediction of mean discharge (Section 7.3) offers the information required to assess whether overtopping is slight, moderate or severe, and make a link to any possible flooding that might result, the prediction of the volumes associated with individual wave events can offer an alternative (and often more appropriate) measure for the assessment of tolerable overtopping levels and possible direct hazard. First, a method is given for the prediction of maximum overtopping volumes expected associated with individual wave events for plain vertical structures under perpendicular wave attack (Section 7.4.2). This method is then extended to composite (bermed) structures (Section 7.4.3) and to conditions of oblique wave attack (Section 7.4.4). Finally, a short section on scale effects is included (Section 7.4.5). Also refer to Section 4.2.2.

The methods given for perpendicular wave attack are the same as those given previously in UK guidance (EA/Besley, 1999). Only the extension to oblique wave attack is new.

7.4.2 Overtopping volumes at plain vertical walls

The first step in the estimation of a maximum expected individual wave overtopping volume is to estimate the number of waves overtopping (N_{ow}) in a sequence of N_w incident waves.

For **non-impulsive conditions**, this was found to be well-described by (Franco et al., 1994)

$$N_{ow} = N_w \exp\left\{-1.21\left(\frac{R_c}{H_{m0}}\right)^2\right\} \quad (\text{for } h_* > 0.3) \qquad 7.23$$

(arising from earlier tests on sloping structures in which situation the number of overtopping waves was directly linked to run-up, in turn linked to a Rayleigh-distributed set of incident wave heights).

Under **impulsive conditions**, N_{ow} is better described by (EA/Besley, 1999)

$$N_{ow} = 0.031 N_w \times \frac{H_{m0}}{h_* R_c} \qquad (\text{for } h_* > 0.3) \qquad 7.24$$

where $h_* R_C / H_{m0}$ is the dimensionless freeboard parameter for impulsive conditions (Equation 7.1).

The distribution of individual overtopping volumes in a sequence is generally well-described by a two-parameter Weibull distribution (also refer to Section 4.2.2);

$$P_V = 1 - \exp\left\{-\left(\frac{V}{a}\right)^b\right\} \qquad 7.25$$

where P_V is the probability that an individual event volume will not exceed V. a and b are Weibull "shape" and "scale" parameters respectively. Thus, to estimate the largest event in a

wave sequence predicted to include (*e.g.*) N_{ow} = 200 overtopping events, V_{max} would be found by taking P_V = 1/200 = 0.005. Equation 7.25 can then be rearranged to give

$$V_{\max} = a\,(\ln N_{ow})^{1/b} \qquad 7.26$$

The Weibull shape parameter a depends upon the average volume per overtopping wave V_{bar} where

$$V_{bar} = \frac{qT_{m-1,0}\,N_w}{N_{ow}} \qquad 7.27$$

For *non-impulsive conditions*, there is a weak steepness-dependency for the scale and shape parameters *a* and *b* (FRANCO (1996));

$$a = \begin{cases} 0.74V_{bar} \\ 0.90V_{bar} \end{cases} \qquad b = \begin{cases} 0.66 & \text{for } s_{m-1,0} = 0.02 \\ 0.82 & \text{for } s_{m-1,0} = 0.04 \end{cases} \qquad (\text{for } h^* > 0.3) \qquad 7.28$$

For *impulsive conditions*, (EA/BESLEY, 1999; PEARSON et al., 2002);

$$a = 0.92V_{bar} \qquad b = 0.85 \qquad (\text{for } h^* < 0.3) \qquad 7.29$$

The effectiveness of the predictor under impulsive conditions can be gauged from Fig. 7.24.

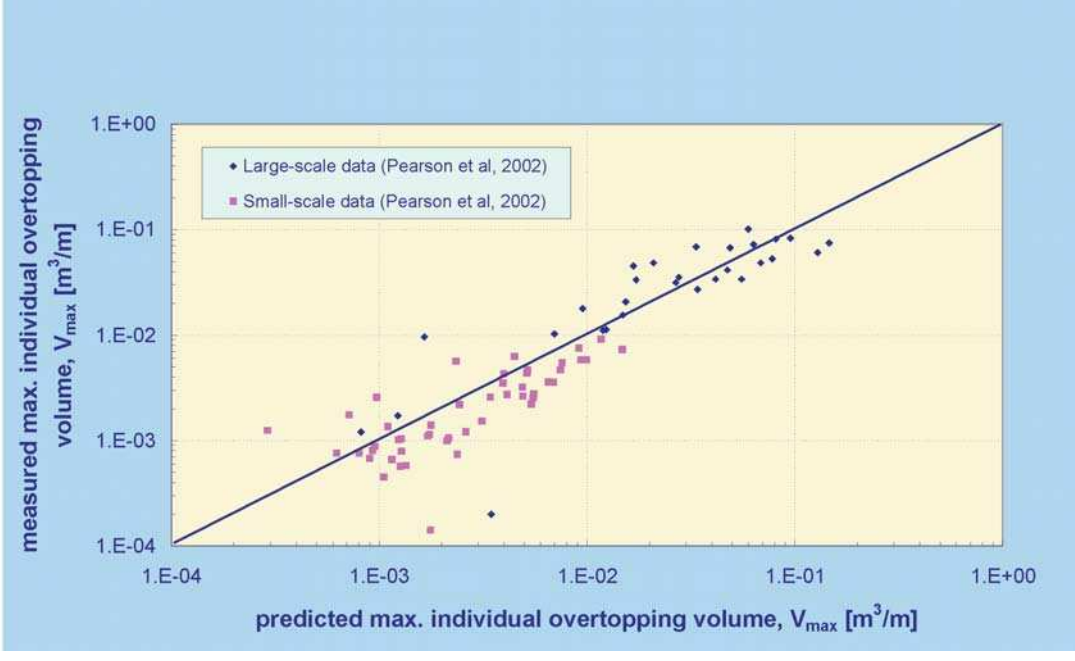

Fig. 7.24: Predicted and measured maximum individual overtopping volume – small- and large-scale tests (PEARSON et al., 2002)

7.4.3 Overtopping volumes at composite (bermed) structures

There is very little information available specifically addressing wave-by-wave overtopping volumes at composite structures. The guidance offered by EA/BESLEY (1999) remains the best available. No new formulae or Weibull *a*, *b* values are known so, for the purposes of maximum overtopping volume prediction, the methods for plain vertical walls (Section 7.4.2) are used. The key discriminator is that composite structures whose mound is sufficiently small to play little role in the overtopping process are treated as *plain vertical*, *non-impulsive*, whereas those with large mounds are treated as *plain vertical*, *impulsive*.

For this purpose, the significance of the mound is assessed using the "impulsiveness" parameter for composite structures, d^* (Equation 7.2). "Small mound" is defined as $d^* > 0.3$, with $d^* < 0.3$ being "large mound".

7.4.4 Overtopping volumes at plain vertical walls under oblique wave attack

For *non-impulsive* conditions, an adjusted form of Equation 7.23 is suggested (FRANCO et al., 1994);

$$N_{ow} = N_w \exp\left\{-\frac{1}{C^2}\left(\frac{R_c}{H_{m0}}\right)^2\right\} \quad \text{(for } h_* > 0.3\text{)} \qquad 7.30$$

C is given by

$$C = \begin{cases} 0.91 & \text{for } \beta = 0^\circ \\ 0.91 - 0.00425\beta & \text{for } 0^\circ < \beta < 40^\circ \\ 0.74 & \text{for } \beta \geq 40^\circ \end{cases} \quad \text{(for } h_* > 0.3\text{)} \qquad 7.31$$

For *impulsive conditions* (as determined for perpendicular i.e. $\beta = 0°$ wave attack), the procedure is the same as for perpendicular ($\beta = 0°$) wave attack, but different formulae should be used for estimating the number of overtopping waves (N_{ow}) and Weibull shape and scale parameters – see Table 7.2 (NAPP et al., 2004).

Table 7.2: Summary of prediction formulae for individual overtopping volumes under oblique wave attack. Oblique cases valid for $0.2 < h^* Rc / H_{m0} < 0.65$. For $0.07 < h^* R_c / H_{m0} < 0.2$, the $\beta = 0^0$ formulae should be used for all β

β = 15°	β = 30°	β = 60°
$N_{ow} = 0.01\, N_w \times \left(\frac{H_{m0}}{h_* R_c}\right)^{-1.6}$	$N_{ow} = 0.01\, N_w \times \left(\frac{H_{m0}}{h_* R_c}\right)^{-1.4}$	treat as non-impulsive
$a = 1.06\, V_{bar}$	$a = 1.04\, V_{bar}$	treat as non-impulsive
$b = 1.18$	$b = 1.27$	treat as non-impulsive

7.4.5 Scale effects for individual overtopping volumes

Measurements from large-scale laboratory tests indicate that formulae for overtopping volumes, based largely upon small-scale physical model studies, scale well (Fig. 7.24) (PEARSON et al., 2002). No data from the field is available to support "scale-ability" from large-scale laboratory scales to prototype conditions.

7.5 Overtopping velocities, distributions and down-fall pressures

7.5.1 Introduction to post-overtopping processes

There are many design issues for which knowledge of just the mean and/or wave-by-wave overtopping discharges/volumes are not sufficient, e.g.

- assessment of direct hazard to people, vehicles and buildings in the zone immediately landward of the seawall;
- assessment of potential for damage to elements of the structure itself (e.g. crown wall; crown deck; secondary defences);

The appreciation of the importance of being able to predict more than overtopping discharges and volumes has led to significant advances in the description and quantification of what can be termed "post-overtopping" processes. Specifically, the current state of prediction tools for

- the speed of an overtopping jet (or "throw velocity");
- the spatial extent reached by (impulsive) overtopping volumes, and
- the pressures that may arise due to the downfalling overtopped jet impacting on the structure's crown deck.

7.5.2 Overtopping throw speeds

Studies at small-scale based upon video footage (Fig. 7.25) suggest that the vertical speed with which the overtopping jet leaves the crest of the structure (u_z) may be estimated as

$$u_z \approx \begin{cases} 2 \text{ to } 2.5 \times c_i & \text{for non-impulsive conditions} \\ 5 \text{ to } 7 \times c_i & \text{for impulsive conditions} \end{cases} \qquad 7.32$$

where $c_i = \sqrt{gh_s}$ is the inshore wave celerity (BRUCE et al., 2002).

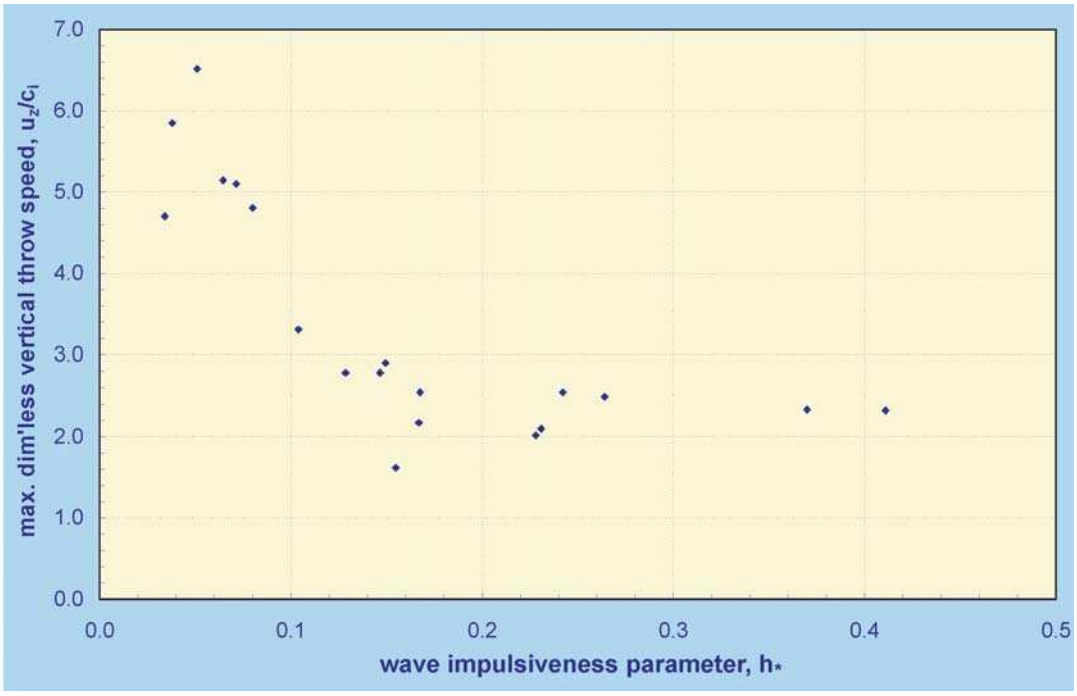

Fig. 7.25: Speed of upward projection of overtopping jet past structure crest plotted with "impulsiveness parameter" h_* (after BRUCE et al., 2002)

7.5.3 Spatial extent of overtopped discharge

The spatial distribution of overtopped discharge may be of interest in determining zones affected by direct wave overtopping hazard (to people, vehicles, buildings close behind the structure crest, or to elements of the structure itself).

Under green water (non-impulsive) conditions, the distribution of overtopped water will depend principally on the form of the area immediately landward of the structures crest (slopes, drainage, obstructions etc.) and no generic guidance can be offered (though see Section 7.5.2 for information of speeds of overtopping jets).

Under violent (impulsive) overtopping conditions, the idea of spatial extent and distribution has a greater physical meaning – where does the airborne overtopping jet come back to the level of the pavement behind the crest? The answer to this question however will (in general) depend strongly upon the local wind conditions. Despite the difficulty of directly linking a laboratory wind speed to its prototype equivalent (see Section 7.3.6) laboratory tests have been used to place an upper bound on the possible wind-driven spatial distribution of the "fall back to ground" footprint of the violently overtopped volumes (PULLEN et al., 2004 and BRUCE et al., 2005). Tests used large fans to blow air at gale-force speeds (up to 28 ms^{-1}) *in the laboratory*. The resulting landward distributions for various laboratory wind speeds are shown in Fig. 7.26. The lower (conservative) envelope of the data give the approximate guidance that 95 % of the violently-overtopped discharge will land within a distance of $0.25 \times L_o$, where L_o is the offshore (deep water) wavelength.

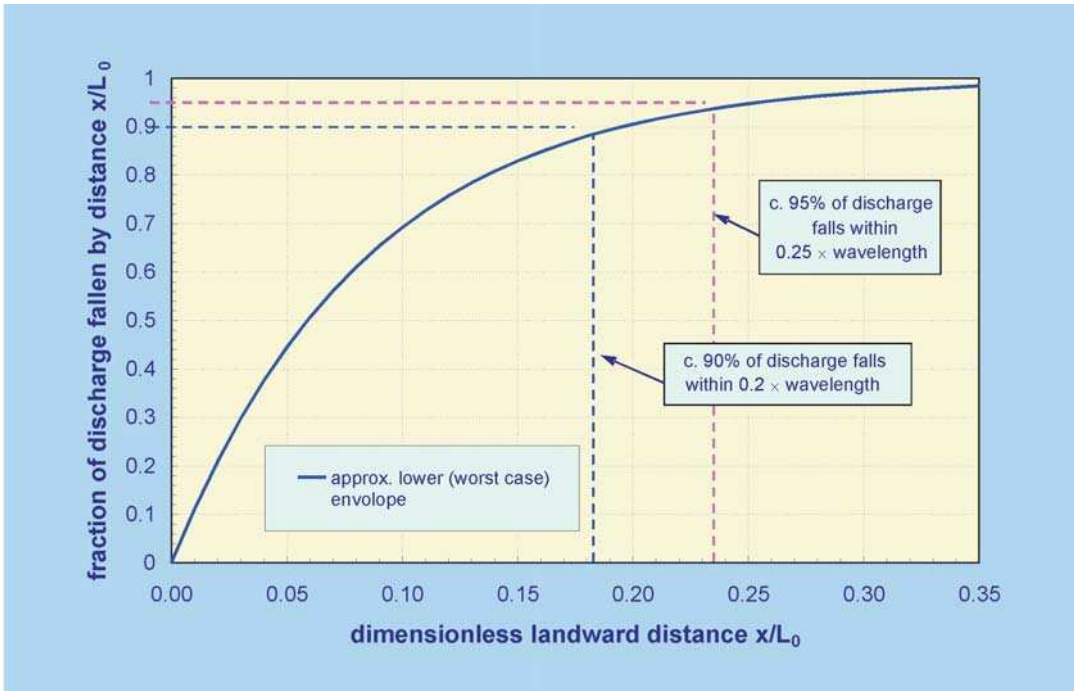

Fig. 7.26: Landward distribution of overtopping discharge under impulsive conditions. Curves show proportion of total overtopping discharge which has landed within a particular distance shoreward of seaward crest

7.5.4 Pressures resulting from downfalling water mass

Wave impact pressures on the crown deck of a breakwater have been measured in small- and large-scale tests (BRUCE et al., 2001; WOLTERS et al., 2005). These impacts are the result of an impacting wave at the front wall of the breakwater generating an upwards jet which in turn falls back onto the crown deck of the structure. Small-scale tests suggest that local impact pressure maxima on the crown deck are smaller than *but of the same order of magnitude* as wave impact pressures on the front face. For high-crested structures ($R_c / H_{m0} > 0.5$), pressure maxima were observed to occur within a distance of ~ 1.5 × H_{m0} behind the seaward crest. For lower-crested structures (R_c / H_{m0} < 0.5) this distance was observed to increase to ~ 2 × H_{m0}. Over all small-scale tests, pressure maxima were measured over the range

$$2 < \frac{p_{1/250}}{\rho g H_{m0}} < 17 \qquad \text{with a mean value of 8} \qquad 7.33$$

The largest downfall impact pressure measured in large-scale tests was 220 kPa (with a duration of 0.5 ms). The largest downfall pressures were observed to result from overtopping jets thrown upwards by very-nearly breaking waves (the "flip through" condition). Although it might be expected that scaling small-scale impact pressure data would over-estimate pressure maxima at large scale, approximate comparisons between small- and large-scale test data suggest that the agreement is good.

7.6 Uncertainties

Wave overtopping formulae for vertical and steep seawalls depend on the type of wall which is overtopped and the type of wave breaking at the wall. The wave overtopping formulae used are however similar to the ones used for sloping structures such as dikes and rubble mound structures. Therefore, again the same procedure is suggested as used already for Sections 5.7 and 6.3.7.

The uncertainty in crest height variation for vertical structures is different from sloping structures and should be set to about 0.04 m. All uncertainties related to waves and water levels will remain as discussed within Section 5.7. Similarly, the results of these additional uncertainties have little influence on the results using the model uncertainty only. This is evident from (e.g.) Fig. 7.10 for impulsive conditions at a plain vertical wall.

Resulting probabilistic and deterministic design parameters are summarised in Table 7.3.

Table 7.3: Probabilistic and deterministic design parameters for vertical and battered walls

Type of wall	Type of breaking	Type of formula	Probabilistic par.	Deterministic par.
Plain vertical	non-impulsive	Eq. 7.4	a = 0.04; b = –2.62	a = 0.04; b = –1.80
	impulsive	Eq. 7.6	$a = 1.48 \cdot 10^{-4}$; b = -3.09	$a = 2.77 \cdot 10^{-4}$; b = –3.09
	emergent toe, impulsive	Eq. 7.10	$a = 2.72 \cdot 10^{-4}$; b = –2.69	$a = 3.92 \cdot 10^{-4}$; b = –2.69
Composite	non-impulsive	Eq. 7.4	a = 0.016; b = –3.28	a = 0.016; b = –2.75
	impulsive	Eq. 7.12	$a = 4.10 \cdot 10^{-4}$; b = –2.91	$a = 7.18 \cdot 10^{-4}$; b = –2.91

It is noteworthy that only uncertainties for mean wave overtopping rates have been considered here (as per previous sections dealing with uncertainties). Other methods discussed in this chapter have not been considered per se, but can be dealt with using the principal procedure as discussed in Section 1.5.4.